Stimulation Effects Mapping for Standardizing Coil Placement in Transcranial Magnetic Stimulation

Gangliang Zhong[1, 2], Liang Ma[1,3,4], Yongfeng Yang[5,6,7], Baogui Zhang[1,8,9], Dan Cao[1], Jin Li[1,3], Nianming Zuo[1,3], Lingzhong Fan[1,3,10], Zhengyi Yang[1], Tianzi Jiang[1,3,4,10,11*]

Author affiliations

1 Brainnetome Center, Institute of Automation, Chinese Academy of Sciences, Beijing 100190, China

2 Shanghai Mental Health Center, Shanghai Jiao Tong University School of Medicine, Shanghai 200030, China.

3 National Laboratory of Pattern Recognition, Institute of Automation, Chinese Academy of Sciences, Beijing 100190, China

4 School of Artificial Intelligence, University of Chinese Academy of Sciences, Beijing 100190, China

5 Department of Psychiatry, Henan Mental Hospital, The Second Affiliated Hospital of Xinxiang Medical University, Xinxiang 453002, China

6 Henan Key Lab of Biological Psychiatry, Xinxiang Medical University, Xinxiang 453002, China

7 International Joint Research Laboratory for Psychiatry and Neuroscience of Henan, Xinxiang 453002 China

8 State Key Laboratory of Brain and Cognitive Sciences, Beijing MRI Center for Brain Research, Institute of Biophysics, Chinese Academy of Sciences, Beijing, China

9 University of Chinese Academy of Sciences, Beijing, China

10 Center for Excellence in Brain Science and Intelligence Technology, Institute of Automation, Chinese Academy of Sciences, Beijing 100190, China

11 Research Center for Augmented Intelligence, Zhejiang Lab, Hangzhou 311100, China

***Address correspondence to**: jiangtz@nlpr.ia.ac.cn

Running title: Transcranial mapping stimulation effects of TMS

Abstract

Transcranial magnetic stimulation (TMS) is a well-established non-invasive technique used to investigate brain function in health and disease. However, conventional methods of coil placement have limitations in accurately estimating the effects of TMS. Numerical modeling has shown promise in optimizing coil placement by providing a means to quantify the relationship between coil placement and region-specific electric field (E-field) effects. In this context, we propose the Stimulation Effects Mapping (SEM) framework to address this issue. The SEM framework aims to quantify It has been validated using diverse samples and neuroimaging data, allowing for standardized individual coil placements and optimal group-level positions. Through the analysis of a large dataset consisting of 5 million E-field modeling results from 212 participants, SEM consistently quantified the relationship between coil placement and region-specific E-field effects. In comparison to conventional methods and recent techniques, SEM-based optimal coil placement offers the same convenience while providing an improved understanding of depression treatment efficacy. By accurately quantifying the relationship between coil placement and E-field effects, SEM enables the identification of optimal coil positions that target specific cortical regions. This advancement in coil placement standardization overcomes limitations and promotes the precise modulation of brain activity based on E-field stimulation effects. The open-source nature of the SEM framework facilitates its adoption and encourages the precise modulation of brain activity through E-field stimulation. By leveraging the SEM framework, transcranial neuromodulation can be advanced, leading to improved outcomes in various applications.

Keywords: Transcranial magnetic stimulation; electric fields; stimulation effects; coil placement; transcranial neuromodulation

1 Introduction

Transcranial magnetic stimulation (TMS) is a well-established non-invasive technique used to investigate brain function in health and disease [1-3]. By applying magnetic pulses to the scalp, TMS can modulate neuronal activity in specific cortical regions, providing valuable insights into brain connectivity and function [4-6]. However, the effectiveness of TMS relies heavily on precise coil placement (position and orientation) on the scalp, as the distribution of induced electric fields (E-fields) over the target area varies depending on the placement. Conventional methods for coil placement [7-9] assume a linear relationship between coil position and stimulation effects, neglecting the nonlinear conductivity properties of biological tissue and leading to inconsistent and inconclusive results [10, 11].

To overcome these limitations, numerical modeling has emerged as a promising tool for optimizing TMS coil placement [10-15]. By constructing realistic head models and simulating the induced electric fields (E-fields), numerical modeling enables the estimation of region-specific effects of TMS. This approach allows researchers to analyze the relationship between coil placements and the corresponding target-specific cortical regions. However, accurately quantifying the highly variable relationship between coil placements and region-specific E-field effects remains a challenge. The relationship is influenced by individual anatomical differences, such as skull thickness and conductivity, as well as the orientation and position of the TMS coil. This variable relationship has been revealed by a systematical numeric study [16], which simulated E-fields-induced distributions for thousands of coil placements. However, accurately quantifying the highly variable relationship between large-scale coil placements and stimulation effects across individuals or studies is lacking. Existing optimization methods mostly depend on E-field simulations on individuals [17] and cannot develop group optimal settings.

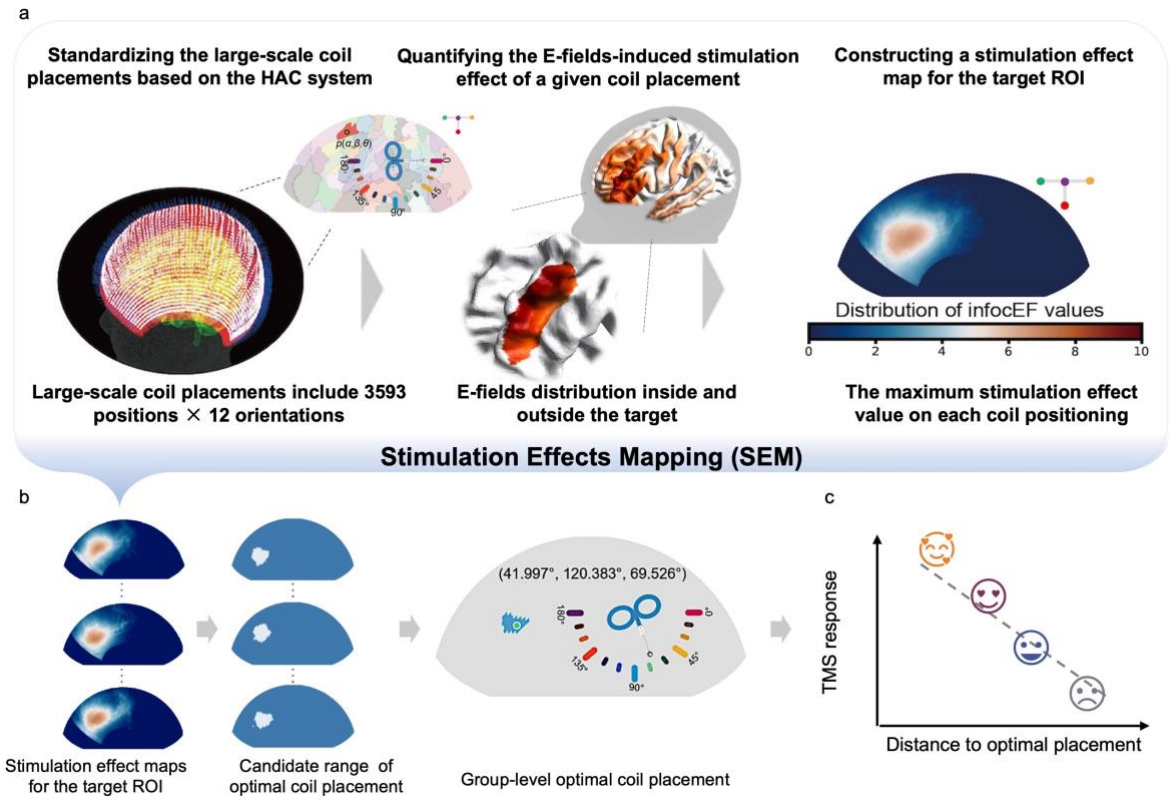

Fig. 1 Schema of the development and validation of the SEM.

Additionally, the process of reconstructing numerical head models and simulating TMS-induced E-fields can be time-consuming, limiting the practicality of this approach [17-19]. Some state-of-the-art methods attempt to improve computation efficiency and reduce costs, such as the ADM method [20], which aims to decrease overall optimization time by reducing the time per E-fields simulation. However, these methods still cannot solve the complex and time-consuming steps of building the head model. The construction of a

head model using a published standard framework takes more than 20 hours [19] and does not include the acquisition of precise neuroimages [17]. Therefore, optimizing coil placements based on E-fields modeling is almost impossible in scientific or clinical applications due to the unaffordable computation and time costs involved. A standardized approach to TMS coil placement is needed to develop a generalizable and effective optimization method for group-level coil placements that considers the highly variable relationship between large-scale coil placements and stimulation effects.

In this paper, we propose the Stimulation Effects Mapping (SEM) framework to address these challenges and provide a standardized approach for coil placement optimization (Fig. 1). SEM accurately quantifies the relationship between coil placements and region-specific E-field stimulation effects (Fig. 1a), allowing for the identification of optimal coil placements that effectively target specific cortical regions (Fig. 1b). We validate SEM using diverse samples and neuroimaging data, demonstrating its effectiveness in achieving optimal coil placements at the group level (Fig. 1c). By providing a publicly available SEM framework, we aim to facilitate future coil placement optimization studies and enhance the practicality of TMS in scientific and clinical applications.

2 Materials and Methods

2.1 Subjects

The study included a diverse group of participants, comprising 212 individuals from various datasets. The CASIA dataset consisted of 18 healthy subjects, while the HCP15 dataset included 15 healthy adults. Additionally, the HCP100 dataset comprised 100 healthy adults. The validation datasets consisted of 79 subjects, with 54 subjects from a depression dataset and 25 subjects from a dataset of healthy participants. These datasets were used to evaluate the performance of the optimal coil localization strategy.

2.1.1 CASIA dataset

Subjects. The CASIA dataset included 18 healthy, right-handed subjects with no history of neurological or psychiatric disorders (9 males, age range, 23–31 years; age, 25.28 ± 2.05 years). Written informed consent was obtained from all participants before the scans. The MRI data acquisition was approved by the Ethical Committee of the Institute of Automation, Chinese Academy of Sciences.

Magnetic resonance imaging (MRI) data acquisition. MRI data was acquired using optimized sequences to ensure accurate reconstruction of head models [21]. Individual MR images were acquired with a GE UHP 3.0 T MR scanner: (i) T1-weighted: 342 sagittal slices, matrix size = 340×340, voxel size = 0.7 × 0.7 × 0.7 mm³, flip angle 15°, TR/TE/TI = 4666/4.66/2200 ms (repetition, spin echo, inversion time), (ii) T2-weighted: 324 sagittal slices, matrix size = 360 × 360, voxel size = 0.7 × 0.7 × 0.7 mm³, flip angle 90° TR/TE/TI = 4002/114/1099 ms, (iii) diffusion MRI (dMRI): 96 axial slices, matrix size = 152 × 152, voxel size = 1.5 × 1.5 × 1.5 mm³, TR/TE 10000/52 ms, flip angle 90°, 60 diffusion directions, b-value 1000 s/mm³. An additional b0 image with the reversed encoding direction was acquired and used during the calculation of the anisotropic conductivity sensors for eddy current correction and distortion correction. Technical details are provided in Supplementary table 1.

2.1.2 HCP15 dataset

Subjects and MRI data acquisitions. The HCP15 dataset consisted of MRI data from 15 healthy (10 males, age range, 24–33 years, age, 28.93 ± 2.79 years), and unrelated adults obtained from the Human Connectome Project (HCP) database. These subjects were adopted in this study because the possibility of reconstructing smooth and high-resolution skull and skin surfaces had been verified in [22]. Subject 209733 was abandoned because of an abnormal segmentation of brain tissues. The T1-weighted, T2-weighted, and dMRI images were downloaded in a preprocessed form, following the minimal preprocessing pipeline. The scanning parameters and preprocessing details were specified in previous studies [23, 24].

2.1.3 HCP100 dataset

Subjects and MRI data acquisitions. The HCP100 dataset included MRI data from 100 healthy (39 males, age range, 22–35 years, age, 29.05 ± 3.38 years), and unrelated adults obtained from the HCP database. The T1-weighted and dMRI images were used for the repeatability validation of the SEMs and optimal TMS coil placements. The details of the data acquisition were the same as for the HCP15 dataset.

2.1.4 DP dataset (Depression study)

Participants. Participants in the depression study were recruited from the Second Affiliated Hospital of Xinxiang Medical University. Diagnosis of depression was made based on the Structured Clinical Interview for DSM-IV-TR Axis I Disorders. The severity of depression and anxiety symptoms was assessed using the Beck Depression Inventory (BDI) and Beck Anxiety Inventory (BAI). The study protocol was approved by the Ethics Committees of the hospital, and written informed consent was obtained from all participants. A total of 54 subjects (Han Chinese ancestry, 25 males, age range = 18-55 years, age = 34.15 ± 12.02 years) who completed the treatment were involved in the analysis.

MRI data acquisition. MRI scans were performed using a Siemens Verio 3.0 T MR scanner. The T1-weighted images used in the current study were collected with 192 sagittal slices, matrix size = 256×256, voxel size = 1 × 1 × 1 mm^3, flip angle 7°, TR/TE/TI = 2530/2.43/1100 ms.

TMS strategies for depression treatment. All subjects received TMS treatment sessions using a Magstim Rapid2 stimulator and a Magstim 70 mm figure-of-eight stimulation coil, navigated by a commercial BrainSight system (The Rogue Research Inc.). Stimulation was delivered to the A9/46v cortex at a frequency of 10 Hz. Depression severity was assessed using the BDI and BAI before and after the treatment course.

2.1.5 CASIA II dataset

Participants and MRI data acquisition. The CASIA II dataset included 25 healthy, right-handed individuals (14 males, age range, 24–30 years, age, 25.12 ± 1.88 years). Written informed consent was obtained from all participants before the examination. The T1-weighted image was used for simulating the E-fields distribution, and the details of the MRI data acquisition were the same as the CASIA dataset. The study was approved by the Ethical Committee of the Institute of Automation, Chinese Academy of Sciences.

2.2 SEM building strategy

2.2.1 Definition of the head-anatomy-based coordinates (HAC) system

The HAC system is designed to describe positions on the head and is built using three steps. First, five cranial landmarks inherited from the international 10-20 system [8], the nasion (Nz), inion (Iz), left/right preauricular point (LPA/RPA), and Cz, are calculated based on a population average head model reconstructed by MNI images. Then, these landmarks are transformed into individual image spaces and assigned to the nearest point on the individual scalp. Next, the HAC system is defined using spherical polar coordinates, with the origin at the midpoint of the RPA-LPA line, the O-LPA line as the *x*-axis, the O-Iz line as the *y*-axis, and the O-Cz line as the z-axis. α was the polar angle in the *x*-*y* plane from the *z*-axis with $0 < \alpha < \pi$, and β was the azimuthal angle in the *x*-*y* plane from the x-axis with $0 < \beta < \pi$ of the HAC system. Finally, positions on the scalp surface are parametrized as continuous angle coordinates (α, β) based on the tetrahedrons of the simulation head model.

2.2.2 Definition of the coil placement system

The Coil Placement system is based on the HAC system and allows for the parametrization of coil positions as angle coordinates (α, β). To disperse the coil positions and reduce the number of simulation calculations, a scheme is provided to make sparse and consistent coil placements across individuals. This involves determining points over the scalp based on the angles between specific lines and scaling the number of parts based on the real need. In our case, (i) the angle between the O-Nz line and O-Iz line was separated into 100 equal parts to determine points p_i (i=1, …, 101) over the scalp, then the number of equal parts was scaled to adjust for the real need. (ii) For the left scalp, the angle between the O-LPA line and the O-p_i line was separated into 50 parts to determine points p_{ij} (j=1, …, 51), and the right scalp was done similarly. The coil orientation (θ) is defined as the coil handle orientation when the coil is perpendicular to the location on the scalp. Overall, coil placement can be parametrized as (α, β, θ) based on the HAC system.

2.2.3 Transcranial mapping of stimulation effects

(1) Quantifying the intensity-focality of stimulation effects for targeted ROIs

To simulate the intensity and distribution of the electric field (E-field) in the individual brain, finite element simulation is performed using the SimNIBS software [25] (Supplementary method 2, Supplementary figure 1, 9). The intensity-focality of stimulation effects in targeted regions of interest (ROIs) is quantified using an evaluation function (infocEF). This function identifies the highest intensity of the induced E-field over the targeted ROI while minimally affecting the rest of the brain area. The infocEF values are calculated for each coil placement (α, β, θ) and are used to assess the stimulation effects (Supplementary figure 3).

To concentrate the simulation effects on the target brain region, we calculated the average E-field value of a tetrahedron within the range of the intersection of the boundary of the targeted ROI and a sphere with a 10 mm radius (imitating an effective special range of the TMS modulation) with a center at the center point of the targeted ROI. In our case, the boundaries and centers of the individual targeted ROIs were obtained by a nonlinear transformation of the Brainnetome atlas [26] from standard space (FSL Fnirt, https://fsl.fmrib.ox.ac.uk/fsl/fslwiki). The center point of the targeted ROI had the minimum average distance to the cortical voxels. For a targeted ROI (t), we calculated the value of the intensity ($\mathrm{inEF}_t(\alpha,\beta,\theta)$) and focality ($\mathrm{focEF}_t(\alpha,\beta,\theta)$) of the stimulation effect for each coil placement (α,β,θ) by equation (1) and equation (2), respectively.

$$\mathrm{inEF}_t(\alpha,\beta,\theta) = \frac{\sum_{ROI\cap S} \mathrm{EF}(\alpha,\beta,\theta)}{N_{ROI\cap S}} \tag{1}$$

$$\mathrm{focEF}_t(\alpha,\beta,\theta) = \frac{\sum_{ROI} \mathrm{EF}(\alpha,\beta,\theta)\cdot N_{ROI^{\mathrm{C}}}}{\sum_{ROI^{\mathrm{C}}} \mathrm{EF}(\alpha,\beta,\theta)\cdot N_{ROI}} \tag{2}$$

where *ROI* is a set of tetrahedrons within the range of the targeted ROI and *S* is a set of tetrahedrons within the range of the 10 mm sphere centers at the central point of the targeted ROI, *N* is the number of the subjects in a set and $\mathrm{EF}(\alpha,\beta,\theta)$ is the absolute value of the E-field at each tetrahedron for each coil placement (α,β,θ). If a collection of tetrahedrons within the range of the grey matter are defined as a universal set $\mathbb{U}$, then ROI^{C} is the complement of the ROI set. Then, we calculated the value of the intensity-focality evaluation function ($\mathrm{infocEF}_t(\alpha,\beta,\theta)$) of the stimulation effect for each coil placement (α,β,θ) by equation (3).

$$\mathrm{infocEF}_t(\alpha,\beta,\theta) = \mathrm{a} \times \mathrm{inEF}_t(\alpha,\beta,\theta) + \mathrm{b} \times \mathrm{focEF}_t(\alpha,\beta,\theta) \tag{3}$$

where a and b are constants and their values depend on the weight of $\mathrm{inEF}_t(\alpha,\beta,\theta)$ and $\mathrm{focEF}_t(\alpha,\beta,\theta)$. In the SEM building process, the $\mathrm{inEF}_t(\alpha,\beta,\theta)$ and $\mathrm{focEF}_t(\alpha,\beta,\theta)$, which were calculated based on the data from all the individuals, were separately z-score normalized. We used the z-score normalization to convert the $\mathrm{inEF}_t(\alpha,\beta,\theta)$ data and $\mathrm{focEF}_t(\alpha,\beta,\theta)$ data to a common scale and eliminate their dimensional differences; thus, the value of constants, a and b, were both taken as 1 in our case.

(2) *Transcranial mapping strategy*

The transcranial mapping strategy establishes a quantitative correspondence between intracranial brain space and extracranial coil position using the three degrees of freedom (DOFs) parameters enabled by the HAC system. To illustrate the quantifying process in transcranial mapping, we consider the example of intracranial stimulation effects on a targeted ROI. Each coil placement (α, β, θ) induces a different distribution of the electric field (E-field) in the brain, resulting in distinct infocEF values for the ROI. Thus, the quantitative correspondence consists of the coil placement parameters (α, β, θ) and the corresponding infocEF value ($\mathrm{infocEF}_t$ (α, β, θ)) for the specific targeted ROI.

For each targeted ROI, we store the maximum infocEF value $\mathrm{infocEF}_{max}$ and the corresponding coil orientations $\theta_{max}(s)$ at each location $s(\alpha_s,\beta_s)$, calculated using equation (4). Furthermore, we determined the coil orientations $\theta_{max}(s)$ corresponding to the maximum infocEF for each location were calculated according to equation (5) and stored. For each targeted ROI, this $\mathrm{infocEF}_{max}$ and θ_{max} can be mapped to the coil placement space (Fig. 2b).

$$infocEF_{\max}(s) = infocEF\big(s,\theta_{\max}(s)\big) \tag{4}$$

$$\theta_{\max}(s) = \arg\max\ infocEF(s,\theta) \tag{5}$$

To visualize the intracranial brain information on the scalp surface, we proposed a 3D and 2D side view of the transcranial mapping results (Fig. 2c). Specifically, we virtually flatten the scalp surface within a 2D fan-shaped plane to construct the 2D side view of the entire upper scalp surface, facilitating illustrative analysis.

(3) *Simulation calculations of mapping stimulation effects to large-scale coil placements*

To map the stimulation effects to a large-scale coil placement, we adopted a dispersed coil location approach in the HAC coordinate system to minimize the number of simulations required. This resulted in a total of 43,116 placements, which corresponded to 3593 coil positions. These positions were defined with a 1.8-degree interval of α, a 1.8-degree interval of β, and an approximate 2 mm Euclidean distance between adjacent positions. Additionally, we considered 12 different coil orientations with a 15-degree interval of θ, covering a total of 180 degrees. Across the CASIA, HCP15, and HCP100 datasets, we performed a total of 5,734,428 E-field simulations involving 133 subjects.

The computation cost for the E-fields simulations for 43,116 coil placements was approximately 4,000 cores, with each subject taking 4.5 hours. We utilized 2.5 GHz 2000 Hygon C86 cores, each equipped with 6 GB of RAM.

2.3 Extracting individual-level candidate range for optimizing coil placement

To develop efficient methods for optimizing coil placement, we initially extract a set of potential optimal coil placements at the individual level, known as candidate coil placements (CCP). This process involves utilizing the SEMs of target regions of interest (ROIs) for each individual. We extracted the CCPs $(\alpha_{CCP}(t), \beta_{CCP}(t), \theta_{CCP}(t))$ based on the 85% threshold of the maximum infocEF value in each targeted ROI (eq. 6-7), as depicted in Figure 2c.

$$\mathrm{CCP} = \left\{\left(\mathrm{s}_{CCP}, \theta_{max}(\mathrm{s}_{CCP})\right) \mid \forall \mathrm{s}_{CCP}: \mathrm{infocEF}_{max}(\mathrm{s}_{CCP}) \geq 0.85 \times \mathrm{infocEF}_{max}(\mathrm{s}_{max})\right\} \quad (6)$$

$$\mathrm{s}_{max} = \arg\max \mathrm{infocEF}_{max}(\mathrm{s}) \quad (7)$$

To ensure the reliability of our method, we selected 76 cortical targets with diverse neuroanatomy. The boundaries and centers of the cortical brain areas were defined using the Human Brainnetome Atlas [26]. When selecting the cortical targets, we excluded areas where the distance between the scalp and cortex exceeded 40 mm, considering the effective penetration depth of the TMS coil.

2.4 Constructing a group-level optimal placement of TMS coils

To create the optimal coil placement at the group level, we utilized the set of potential optimal coil placements and the optimal coil placement for each target ROI. By aggregating the candidate coil position sets among individuals, we calculated the center of gravity of the distributions of the aggregative group-level coil placements.

To achieve this, we first mapped all the individual candidate coil placements (CCPs) of the same targeted ROI into a common coil placement system (α, β, θ). In this system, each coil placement $(1.8 \times 1.8 \times 15°)$ was covered by either none, a single, or multiple CCPs. We then determined the frequency of each coil location based on the individual CCPs. The aggregation of the CCPs (ACCP) $(\alpha_{ACCP}(t), \beta_{ACCP}(t), \theta_{ACCP}(t))$ for each targeted ROI was defined by extracting the coil positions whose frequency was above 95%. These ACCPs can be visualized in the 2D side view of the localization space (Fig. 4a).

Next, we calculated the population probability (p) for each coil location in the ACCP, resulting in a distribution of heat values for the included coil placements $[m]$ (combination of $i \times j$ locations and k coil rotations). The optimal coil placement was estimated by calculating the center of gravity (CoG) of the included coil placements combined with the population probability (p_m), using the following equations (8-10):

$$\alpha_{\mathrm{OPA}} = \frac{\sum_{ACCPs} \alpha_{\mathrm{i}} p_i}{\sum_{ACCPs} p_i} \quad (8)$$

$$\beta_{\mathrm{OPA}} = \frac{\sum_{ACCPs} \beta_{\mathrm{j}} p_j}{\sum_{ACCPs} p_j} \quad (9)$$

$$\theta_{\mathrm{OPA}} = \arg\max\ infocEF(\alpha_{\mathrm{OPA}}, \beta_{\mathrm{OPA}}, \theta_k) \qquad (10)$$

We stored the set of potential optimal coil placements at the group level, along with their optimal location (α_{opt}, β_{opt}) and optimal coil orientation θ_{opt}. These data can be visualized in the 2D side view of the localization space, as depicted in Fig. 4b.

By applying this approach, we obtained the group-level optimal coil placement, which provides valuable insights for optimizing TMS coil placement in a standardized manner at the group level.

2.5 Statistics

Statistics were performed using several Python packages, including scipy, sklearn, and statsmodels. The exact sample values and results of statistical tests can be found in the figure captions or within the figure panels themselves. Statistical significance was determined at $p < 0.05$.

2.5.1 Leave-one-out cross-validation strategy

To validate the stability and consistency of the optimal coil placement, we utilized a leave-one-out cross-validation strategy. This approach involved constructing optimal coil placements using n-1 subjects and then validating them on the left-out subject. This process was repeated n times to cover the entire cohort. Essentially, for each subject, a new optimal coil placement was generated based on the remaining subjects, allowing us to assess the reliability and robustness of the placement algorithm.

2.5.2 Dice index for similarity of candidate coil positions

In Fig. 4e, we calculated the Dice index to quantify the similarity of the candidate coil positions for 72 targeted ROIs in OPAs built using the leave-one-out cross-validation method. Additionally, we computed the average Dice index values between 18 OPAs.

2.5.3 Euclidean distance and average optimal coil position

Fig. 4f presents the Euclidean distance between the average optimal coil position and the nearest scalp site of the targeted ROI. The average optimal coil position represents the mean value of the optimal coil positions in OPAs built using the leave-one-out cross-validation method.

2.5.4 Treatment response analysis

In Fig. 5, we investigate the relationship between treatment response rates and stimulation distances. We conduct a Pearson correlation analysis (Fig. 5b, c) to assess this relationship and perform regression analysis (Fig. 5e, f) to investigate the variation in treatment response rates with stimulation distances. These analyses utilize Python packages such as scipy.stats and sklearn.linear.

2.5.5 E-fields distribution analysis

Fig. 6 involves computing the E-fields distribution for each subject based on the coil placements obtained from the NS, OPA, and ADM methods. We use the Kruskal-Wallis H-test to examine significant differences in the z-scored average E-field normal component (E-norm) values within the targeted region among the three methods at the group level. Additionally, we conduct post-hoc tests using the Dunn-Bonferroni method to identify specific pairwise differences if the overall test is significant. For these non-parametric analyses, we employ Python packages such as scipy.stats.mannwhitneyu and statsmodels.stats.multitest.

2.5.6 Focality score for population consistency

We developed a focality score (FS) in Supplementary Fig. 5a to evaluate the population consistency of each targeted ROI. FS is defined as the ratio of the coincidence locations set in the Candidate Coil Placement (CCP) of all individuals between 80% and 50%.

2.5.7 Comparison of FS values

Supplementary Fig. 5b compares the difference between the FS values of our infocEF index and the FS values of a non-focal E-field (nonfocEF) index across 74 targeted ROIs. The nonfocEF index is calculated using equation (12), which sums the E-field (EF) values across all targeted ROIs and divides them by the number of targeted ROIs.

$$\text{nonfocEF}(\alpha,\beta,\theta) = \frac{\sum_{ROI} \text{EF}(\alpha,\beta,\theta)}{N_{ROI}} \quad (12)$$

2.5.8 Efficiency analysis of optimization strategies

Supplementary Fig. 10b evaluates the efficiency of various prior-based optimization strategies. We quantify optimization efficiency using the iteration numbers of the optimization process.

3 Results

3.1 SEM building strategy and workflow

A graphical representation of the three main steps in the SEM approach is provided in Figure 2. It incorporates a 'head-anatomy-based' coordinate (HAC) system (Fig. 2a) to standardize extracranial large-scale coil localizations on the scalp (Fig. 2b) and to map region-relevant E-field stimulation effects to large-scale coil placements (Fig. 2c). The SEM precisely and accurately analyzes the intricate relationship between large-scale coil placements and their biologically meaningful stimulation effects.

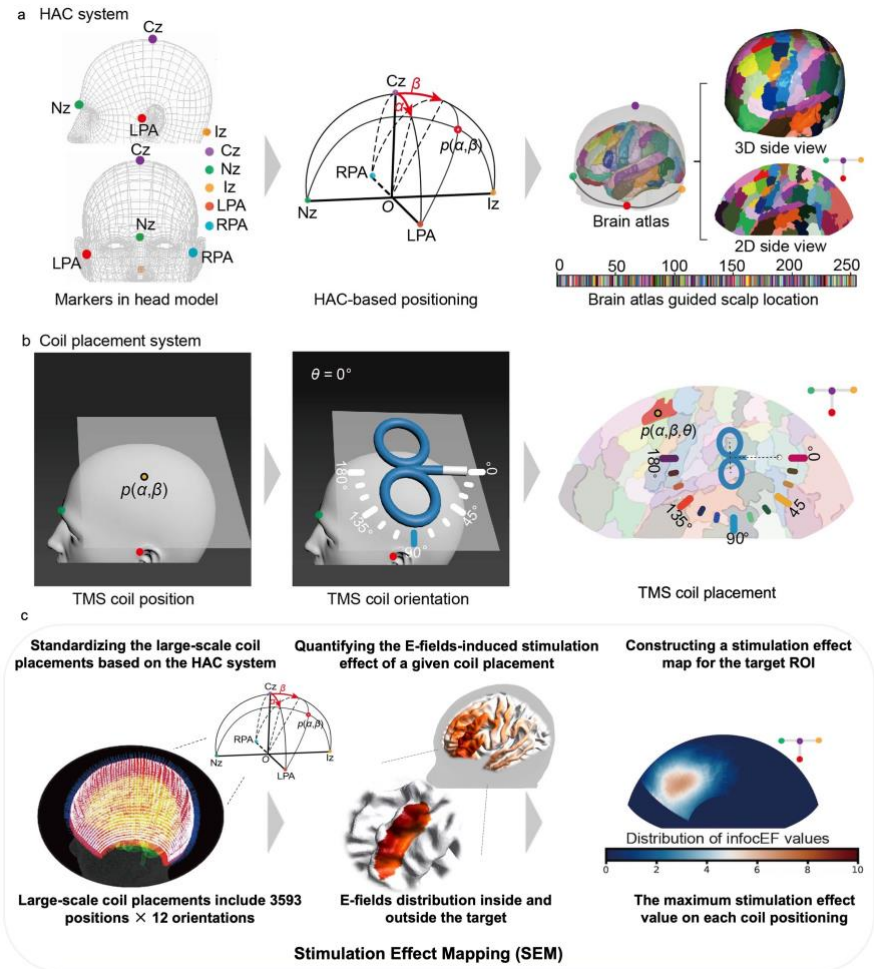

Fig. 2 Building the SEM framework. a, Left panel shows the HAC coordinate system constructed using five cranial landmarks (Nz, Iz, LPA, RPA, Cz) similar to the 10-20 system. The middle panel displays the angle coordinates (α, β) for any site p on the scalp. The right panel shows the mapping of a brain atlas onto the scalp surface, with three-dimensional (3D) and two-dimensional (2D) side views. To target brain regions, we used the Human Brainnetome Atlas as a specific example to provide brain information that could facilitate our general transcranial mapping strategy. A 2D side view of the entire upper scalp surface for the HAC system was created by virtually flattening the scalp surface locations within the 2D fan-shaped plane to aid in the illustrative analysis. b, An overview of the HAC-based coil placement. c, Mapping the stimulation effects of a targeted ROI using a large number of coil placements. The line between point Nz and point Iz is coplanar in the figure, but it is usually not in the same plane as the line between point LPA and point RPA. Top left: A9/46v subregion in the illustrated brain atlas was used as a targeted ROI in this case. Bottom left: 3593 × 12 coil poses used to simulate E-field distributions. Top middle: Distribution of the maximum infocEF values for each coil position. Bottom middle: Distribution of the coil orientations with maximum infocEF for each coil position, plotted as a function of the coil handle orientation. Right: Candidate coil positions and orientations. Candidate coil orientation is shown as polar infocEF

plots. The mean, positive, and negative standard deviation values of infocEF are shown. In the polar infocEF plots, the infocEF values were normalized according to the maximum value of the individual infocEF values.

In the first step, we developed the HAC system to standardize extracranial large-scale coil placements across studies with varying reconstruction precision. The HAC system parametrizes positions on the scalp surface as continuous angle coordinates (α, β) within a range of 0 to 180 degrees. It adapts to dimensional and anatomical differences in cranial shapes and cortical cortexes, distinguishing it from the 10-20 system.

In the second step, based on the HAC system, we provided a TMS coil placement strategy to mathematically define the coil placement. Unlike neuroimage-based strategies that determine coil placement using position (x, y, z coordinates) and orientation (roll, pitch, and yaw) [16, 19], we parametrize the coil placements using angle coordinates (α, β, θ) representing the coil position (α, β coordinates) and orientation (θ coordinate). This reduces the six degrees of freedom (DOFs) of neuroimage coordinates to three DOFs of angle coordinates, simplifying the quantitative description of coil placements. The orientation coordinate is defined as the coil handle orientation when the coil is tangential to the scalp site, ranging from -90 to 90 degrees.

In the third step, SEM enables the mapping of intracranial E-field-induced stimulation effects to extracranial 3 DOFs angle specifications for a large number of coil placements. The SEM framework incorporates the HAC-approved TMS coil placement approach and a quantified approach to E-field-induced stimulation effects. We quantify the intensity and focality of the induced E-field within the targeted cortical regions (infocEF) using human brain atlases. By using the HAC, we map the E-field stimulation effects of a targeted region of interest (ROI) to the corresponding coil placements on the scalp surface for each individual, creating stimulation effect maps (SEMs). The coil placement that maximizes the on-target value of E-field stimulation effects can be considered the optimal choice. SEM allows us to identify the optimal coil position and orientation without specifying a specific stimulation intensity, as the spatial distribution of the E-field is unaffected by its intensity. However, once the optimal coil placement is identified, a range of possible stimulation intensities can be modeled.

The HAC-based transcranial mapping stimulation effects for 43,116 coil placements (3593 positions × 12 orientations) took approximately 2 minutes per subject to compute on a workstation with an Intel Core i9-9880H CPU and 32G RAM. This demonstrates the computational efficiency and feasibility of the SEM framework in practical applications.

3.2 SEM enhances the robustness and consistency of coil placements

To accurately map intracranial E-fields-induced effects to extracranial coil placements using SEM, it is crucial to assess the robustness and consistency of the core HAC system across individuals and datasets. We hypothesized that using the HAC system to obtain coil locations would be consistent across individuals. To validate this hypothesis, we divided the scalp into regions based on percentages of the total front-back and right-left angles, similar to the International 10-20 system. We evaluated the consistency of obtained coil positions across different individuals and compared them with positions obtained using conventional coil placement methods (Fig. 3a). Conventional coil placement methods, such as the commonly used “5-cm” rule which has U.S. Food and Drug Administration approval [27-29] and the International 10-20 system endorsed by the Clinical TMS Society [7, 30, 31] are based on scalp-surface-based coordinate (SSC) system, which relies on the measurement of the distance between specific landmarks on the scalp.

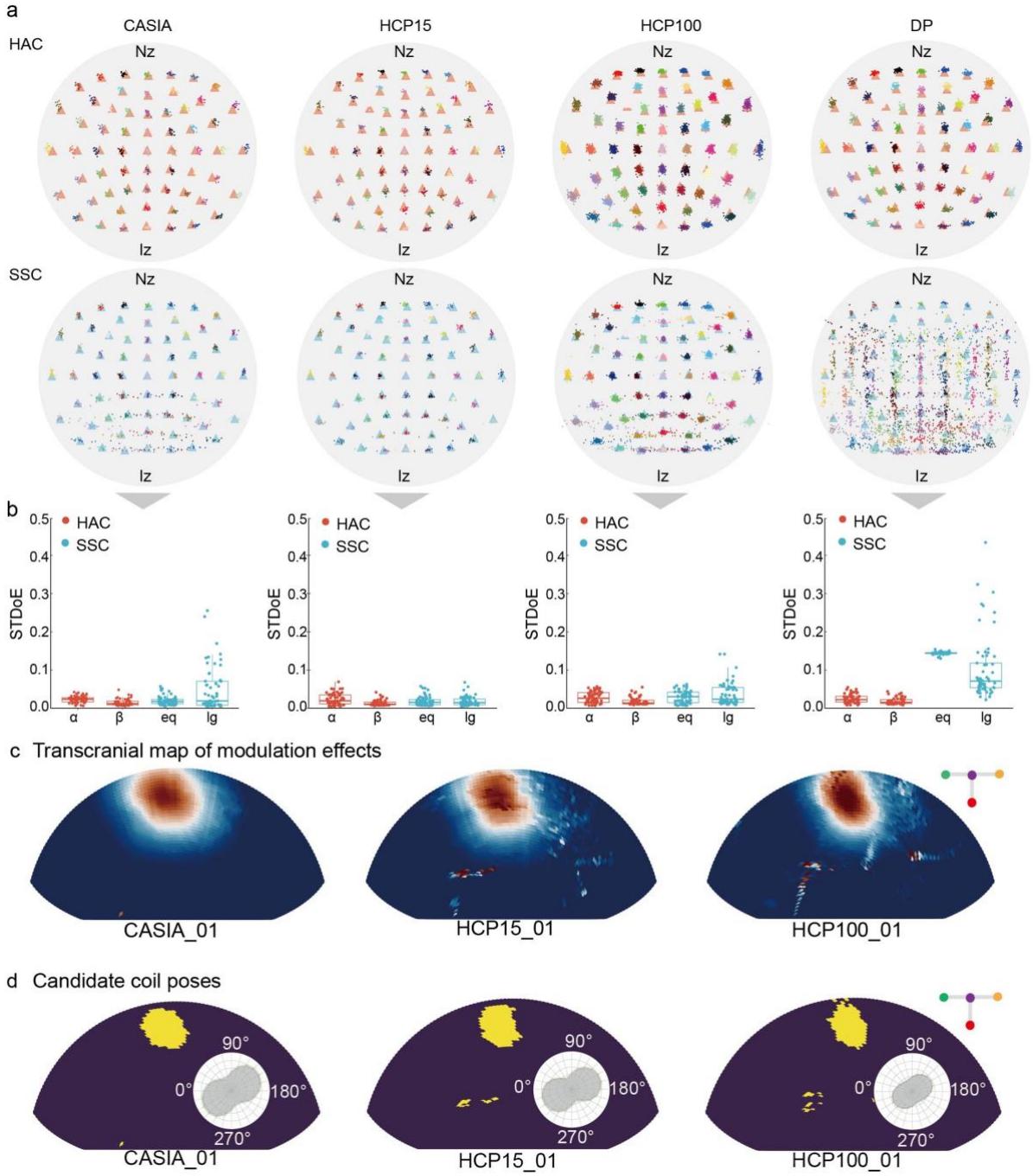

Fig. 3 Transcranial mapping performance of SEM. a, Individual distributions of the reference points in the 10-20 system, constructed using the HAC and SSC systems. Each point corresponds to an individual reference point, with different colors used for different reference points to facilitate visual differentiation. b, Quantitative evaluation of the location errors of the two different systems, in terms of the STDoE for each reference point in the 10-20 system. Box plot: the center line represents the median, while the box limits indicate the upper and lower quartiles. The whiskers represent 1.5 times the interquartile range, and the points indicate the STDoE value for each reference point. c, SEMs of the A9/46v targeted subregion for the first subject in the CASIA, HCP15, and HCP100 datasets. d. Candidate coil placements extracted from the SEMs shown in Fig. 3c.

The HAC reference points consistently exhibited tight distributions across the datasets, while the SSC reference points showed greater variability, particularly in datasets with lower reconstruction accuracy and surface smoothness (Fig. 3a). The HAC system demonstrated quantitative robustness compared to the SSC system in terms of consistency across individual positions. The standard deviation of errors (STDoE) between the population average and individual positions for each reference point of the 10-20 system was lower with the HAC system (Fig. 3b). The HAC system demonstrated strong agreement across the four datasets, with STDoE values below 10% for the locations of α and β. In contrast, the SSC system's STDoE values varied between datasets and only fell below 10% for the HCP15 dataset with high reconstruction accuracy. These findings suggest that conventional scalp-surface-based methods are less effective in

accurately quantifying coil placements, while the HAC system provides greater reliability in localizing TMS coils across individuals and datasets.

We also constructed SEMs for three independent datasets (CASIA, HCP15, and HCP100) to evaluate the performance of the HAC system in mapping E-fields-induced stimulation effects. Our results demonstrate that the distribution of stimulation effects can vary depending on individual-specific cranial dimensions and neuroanatomy (Fig. 3c, Supplementary figure 1). However, the distribution of candidate coil placements was similar for the three datasets (Fig. 3d), indicating that extracting candidate coil placements effectively eliminates irrelevant placements for further analysis. By defining a candidate set of coil locations and orientations based on stimulation effects, it is possible to optimize individual or group-level coil placement.

In summary, this analysis revealed the reproducibility and robustness of the SEM-based transcranial mapping strategy for localizing TMS coils.

3.3 Performance of optimizing coil placements based on SEMs

To evaluate the performance of our coil placement optimization method based on SEMs, we focused on the A9/46v subregion in Brainnetome atlas [26] within the CASIA dataset. By constructing SEMs for all individuals, we derived candidate sets of coil locations and orientations, which exhibited high consistency (Fig. 4a, Supplementary figure 3-4).

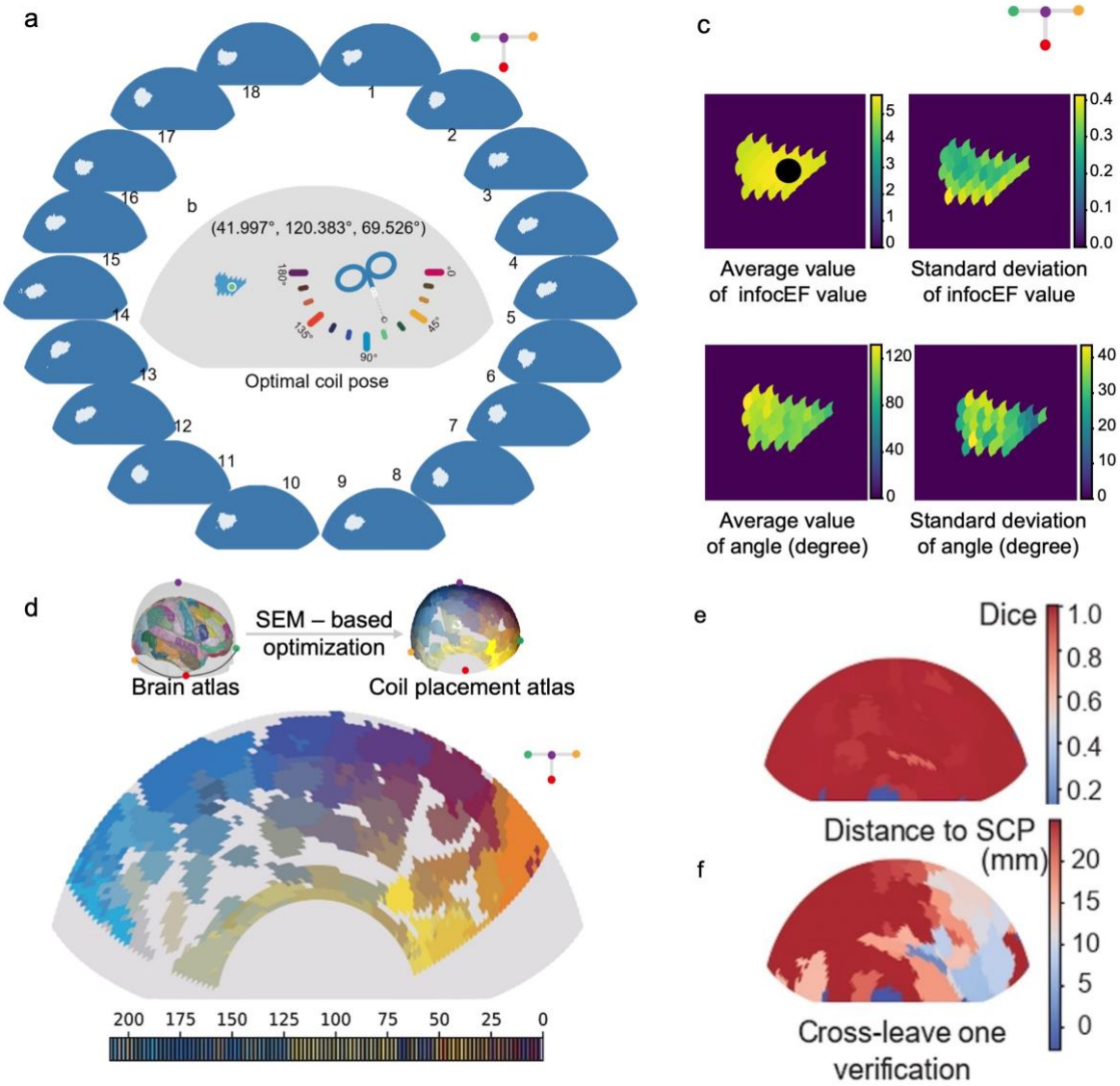

Fig. 4 Optimization of coil placements facilitated by SEM. a, Candidate coil locations for A9/46v subregion targeted in all subjects (n = 18) in the CASIA dataset. b, Aggregative coil locations and optimal coil placement for targeted A9/46v subregion. c, The top left panel shows the average infocEF values at each site of the aggregative coil locations, the top right panel shows the standard deviation of infocEF values at each site of the aggregative coil locations, the bottom left panel shows the average coil angles at each site of the aggregative coil locations, and the bottom right panel shows the standard

deviation of the coil angles at each aggregative coil location site. d, Aggregate of candidate coil locations for 74 targeted ROIs. e, Dice coefficient of the aggregative coil locations calculated using the leave-one-out cross-validation method. f, Euclidean distance (ED) between optimal coil position and the nearest scalp site for 74 targeted ROIs.

The optimal coil placement for the A9/46v targeted subregion was determined to be (41.997°, 120.383°, 69.526°) (Fig. 4b), which corresponds to MNI coordinates of -60 mm, 56 mm, and 27 mm, along with a corresponding optimal coil orientation of 69.526°. The infocEF values and coil angles around the optimal coil position exhibited small standard deviations, further demonstrating consistency (Fig. 4c).

We also tested the replicability of the aggregation analysis for 76 cortical targets with heterogeneous neuroanatomy (Fig. 4d, Supplementary figure 6-7). Our method consistently produced optimal coil location across individuals for all targets (Supplementary figure 5a). In almost 77.63% of the targeted ROIs, the infocEF method (target-specific E-fields stimulation effects) outperformed the roiEF (non-target-specific E-fields stimulation effects), showing a significantly higher focality score (P = .011) (Supplementary Figure 5b).

Furthermore, we assessed the spatial correspondence between aggregations of coil positions calculated by the leave-one-out cross-validation method, measuring the Dice coefficient (DC) (Fig. 4e). The strong spatial similarity observed indicates the consistency and spatial similarity of the aggregative coil positions, validating the viability of our SEM for calculating optimal coil placements in any target ROI. Additionally, we compared the Euclidean distance (ED) between the optimal coil position calculated by the leave-one-out cross-validation method and an alternative coil position commonly used in neuroimage-based localization, which is the nearest scalp site to the target (Fig. 4f). The ED results revealed significant differences between the two methods, emphasizing the importance and necessity of incorporating the nonlinear relationship between coil placements and stimulation effects in SEMs.

In conclusion, our SEM approach provides a reliable and robust method for optimizing coil placement in transcranial mapping studies. The high consistency, low standard deviations, and spatial similarity observed in the results demonstrate the effectiveness of our method in achieving stable and optimal group positions for coil placements.

3.4 Evaluating the clinical interpretability of optimal coil position from SEM-based

To evaluate the clinical interpretability of the optimal coil position obtained from the SEM-based method, we compared its performance with an alternative E-field-based optimizing algorithm known as the fast computational auxiliary dipole method (ADM). The ADM method involves building a simulation model based on individual neuroimages and inferring the optimal coil position. While the ADM method offers the advantage of quickly inferring optimal coil placement, it still requires a substantial amount of time for model building and simulation calculations [20]. In contrast, the SEM method does not involve the process of building a simulation model and requires no further calculations once the optimal coil position is generated, making it more efficient for determining the group-level optimal placement.

To investigate the clinical interpretability of optimized coil position based on E-fields-induced stimulation effects, we conducted a retrospective study of 54 patients with depression. Previous studies have shown the effectiveness of neuromodulation based on induced E-field effects [13-15], which suggests that the distance between the optimal coil position and the real stimulation site may affect the antidepressant outcomes (% change in BDI relative to pre-rTMS BDI or %ΔBDI). The A9/46v subregion in the Brainnetome atlas was selected as the targeted cortical region, based on its functional and structural connections with the anterior cingulate cortex, which is widely recommended for TMS treatment of depression [9]. The treatment initially involved localizing the coil at the nearest scalp site of the targeted cortical ROI without considering E-fields-induced stimulation effects.

We found a significant relationship between the treatment response and the distance between the optimal coil position in the SEM-based method and the real stimulation site (Distance_{OR}, Fig. 5a) (P = .0243) (Fig. 5b), indicating that rTMS was most effective for patients with a small Distance_{OR}. In contrast, the distance between the optimal coil position in the ADM method and the real stimulation site (Distance_{AR}) (P = .5473) (Fig. 5c) did not show a significant relationship with the treatment response.

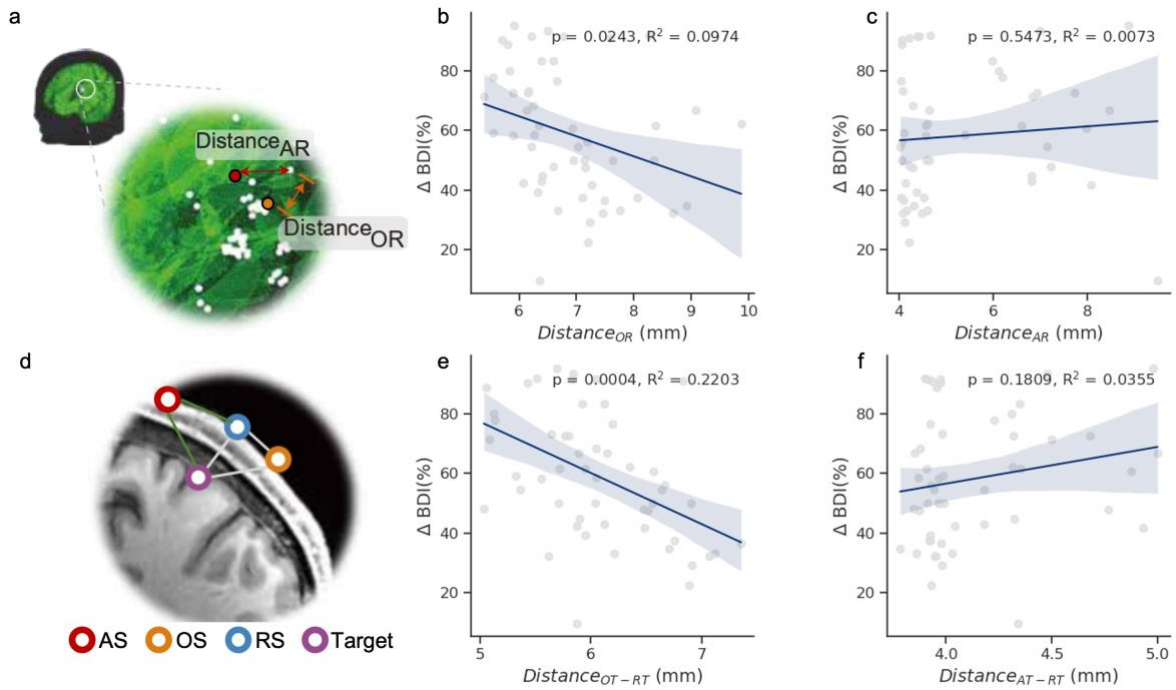

Fig. 5 Relationship between treatment outcomes and coil positions. Distance-related differences in antidepressant outcomes. a, Definition of the distance between the optimal coil position obtained based on SEM and the real stimulation site as Distance_{OR}, and the distance between the optimal coil position in ADM and the real stimulation site as Distance_{AR}. b, Association between Distance_{OR} and differences in antidepressant outcomes (P = .0243). c, Association between Distance_{OR} calculated by an alternative nonfocEF index and differences in antidepressant outcomes (P = .5473). d, Definition of the distance between the real stimulation site and the cortical target site as Distance_{RT}, the distance between the optimal coil position obtained based on SEM and the cortical target site as Distance_{OT}, and the distance between the optimal coil position in ADM and the cortical target site as Distance_{AT}. e, Association between the difference in Euclidian distance of the optimal coil position and the targeted ROI and the Euclidian distance of the real stimulation site and the targeted cortex (Distance_{OT-RT}) with differences in antidepressant outcomes (P = .0004). f, Association between the difference in Euclidean distance of the optimal coil position and the targeted cortex with differences in antidepressant outcomes (P = .1809).

Furthermore, we investigated whether the distance between the optimal coil position and the real stimulation site could explain the treatment response. Previous research has demonstrated that the Euclidian distance between the real stimulation site and the targeted cortical ROI (Distance_{RT}) can predict treatment response [32, 33]. Using the SEM-based method, we examined the difference between the Euclidian distance for Distance_{OT} and the Distance_{RT}, referred to as $\text{Distance}_{OT\text{-}RT}$ (Fig. 5d). Our findings revealed that $\text{Distance}_{OT\text{-}RT}$ is a significant predictor of treatment response, with an R^2 value of 0.2203 and P value of 0.0004 (Fig. 5e). To further validate our findings, we employed leave-one-out cross-validation on the prediction model of $\text{Distance}_{OT\text{-}RT}$ and %ΔBDI, which resulted in a root mean squared error of 19.2146. In contrast, using the ADM method, the Euclidian distance between the Distance_{AT} and the Distance_{RT}, referred to as $\text{Distance}_{AT\text{-}RT}$, did not show a significant relationship with the treatment response (R^2 = .0355, P = .1809) (Fig. 5f).

These findings provide valuable insights into the potential clinical relevance of the SEM-based method for optimizing coil positioning during TMS treatment.

3.5 Comparison with other TMS coil placement optimizing approaches

We compared the E-field normal component (E-norm) values for the A9/46v targeted region using three different methods: traditional nearest scalp site (NSS), the optimal coil placement provided by the SEM-based method, and the ADM method. The E-norm, which represents the component of the E-fields perpendicular to the cortical surface, is considered crucial for the clinical efficacy of TMS in depression treatment [34]. Our results demonstrate the superiority of the SEM-based over the NSS and ADM methods, as evidenced by significantly higher average E-norm values within the A9/46v targeted region in both the depression dataset and the CASIA II dataset of healthy subjects (Fig. 6a, b).

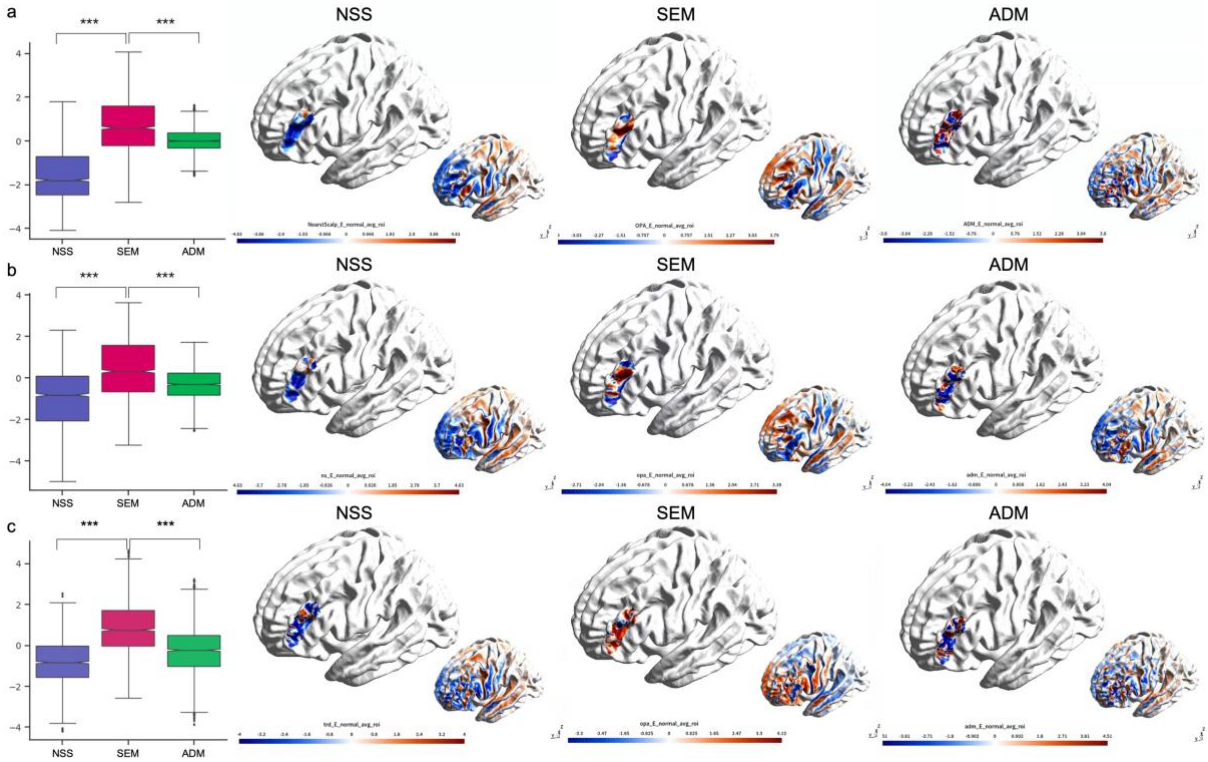

Fig. 6 Comparison of E-field normal component (E-norm) values for targeted regions using traditional nearest scalp site (NSS) and optimal coil placement of SEM and ADM methods. a, Z scores of the E-norm values obtained using the three methods for a depression dataset. The p-values for the comparisons between NSS and SEM, between SEM and ADM, and between NSS and ADM are all less than .001. b, Z scores of the E-norm values obtained using the three methods for a new healthy dataset. The p-values for the comparisons between NSS and SEM, between SEM and ADM, and between NSS and ADM are all less than .001. c, Z scores of the E-norm values obtained using individual optimization strategies based on the three methods. The p-values for the comparisons between NSS and SEM, between SEM and ADM, and between NSS and ADM are all less than .001.

To further illustrate the benefits of the SEM-based method, we conducted a study with fifteen participants from the HCP15 dataset. The goal was to compare the performance of individual optimization strategies based on the traditional NSS, SEM, and ADM methods and highlight the usage and potential advantages of the SEM. The SEM-based method allows users to optimize individual coil placement by incorporating *a priori* knowledge of group-level coil placements, resulting in improved computational efficiency (Supplementary method 1). In contrast, the traditional NSS-based and ADM-based individual optimization strategies lack prior information on optimal coil placements, often requiring simulations of hundreds or even thousands of coil placements to obtain reliable results. Our SEM-based method achieves personalized optimal induced E-fields by simulating fewer than 50 coil placements (Supplementary figure 10). Importantly, the SEM-based individual strategy demonstrated significantly greater stimulation effects compared to the traditional NSS-based and ADM-based individual optimization strategies, as indicated by the higher average E-norm value within the A9/46v targeted region (Fig. 6c).

Taken together, our findings strongly suggest that the SEM-based method is a promising tool for improving the accuracy and efficiency of individual coil placement in TMS studies. It outperforms traditional methods and provides a standardized approach for optimizing coil placement, resulting in enhanced stimulation effects and reduced computational burden. The SEM-based method holds great potential for advancing the field of TMS research and facilitating personalized treatment approaches.

4 Discussion

In this study, we introduced the SEM framework as a solution to the challenges of optimizing TMS coil placements based on induced E-fields effects. The SEM framework offers a systematic approach to quantify the relationship between coil placements and stimulation effects, enabling the mapping of large-scale effects to individual coil placements across different individuals and studies. Our results demonstrate the accuracy and reliability of SEM in quantifying coil placements, as well as its ability to standardize transcranial

mapping across diverse populations and datasets. The robustness of SEM in inferring optimal coil placements across targeted brain regions further highlights its versatility and generalizability.

To facilitate the practical application of SEM in clinical and experimental settings, we generated an optimal coil placement based on high-resolution simulation models. The SEM framework is designed to be compatible with E-field modeling software and coil localizing devices, providing flexibility and generalizability for navigational guidance during coil placement. Our findings suggest that the SEM framework has the potential to significantly advance TMS research and clinical practice by providing a standardized and reliable approach to optimize coil placement for achieving maximum stimulation effects.

4.1 SEM framework enhances transcranial mapping accuracy

The SEM framework, with its incorporation of the HAC system, has demonstrated significant advancements in enhancing the accuracy and reliability of transcranial mapping in neuromodulation. The HAC system addresses the challenges associated with individual-specific cranial dimensions and neuroanatomy, providing a consistent and accurate approach to TMS coil placement on the scalp.

Compared to conventional scalp-surface-based methods, the HAC system offers several advantages. It can handle irregularly reconstructed head models more effectively, enabling more precise localization. Unlike Cartesian coordinate systems used in conventional scalp-surface-based methods [35-39], which rely on scalp curve length proportions and are sensitive to head shapes and perform optimally when the head is an ideal sphere [10, 12, 16, 19, 20, 32, 36, 40, 41], the HAC system is insensitive to the choice of the initial center point, reducing sensitivity to anatomical variations across individuals. The polar coordinate system captures the scale-invariant parameterization of the cortex, facilitating the quantification of anatomically specific stimulation effects. These advantages make the HAC system a more reliable and practical tool for coil placement and transcranial mapping.

Furthermore, the HAC system simplifies the quantitative description of coil placements by reducing the number of parameters and improving computational efficiency for clinical and scientific applications. It also streamlines the process of optimizing coil placement based on large-scale coil placements, increasing accessibility for various neuro-navigation scenarios.

The incorporation of the HAC system into the SEM framework significantly enhances its robustness and accuracy, particularly in situations requiring optimal coil placement for multiple individuals or datasets. This advancement opens new possibilities for precise and effective neuromodulation techniques in fields such as electrical stimulation, focused ultrasound, electroencephalography, and more.

In summary, the HAC system represents a profound contribution to the field of neuromodulation. Its implementation within the SEM framework has improved the accuracy and reliability of transcranial mapping, providing new opportunities for precise and effective neuromodulation techniques.

4.2 SEM-based optimization enhances the repeatability and clinical effectiveness of TMS coil placement

The SEM framework has demonstrated its ability to enhance the repeatability and clinical effectiveness of TMS coil placement optimization. In our study, we confirmed the consistency of SEM-approved coil placement optimization across individuals and multiple targets in the human Brainnetome atlas [26]. This repeatability has important implications for the clinical effectiveness of TMS interventions.

To evaluate the clinical effectiveness of SEM-approved coil placement optimization, we compared our method to conventional neuroimage-based methods and scalp-surface-based methods [reviewed in [9]] in the context of an antidepressant treatment with rTMS. Our optimized coil location, determined by SEM (HAC coordinates: 41.997°, 120.383°; MNI coordinates: -60 mm, 56 mm, 27 mm), was found to be more lateral and anterior compared to conventional methods. These findings align with previous research by Herbsman et al., which also indicated that a more lateral and anterior coil placement is more likely to be effective [32].

In addition, we compared our SEM-based method with the ADM method and found that stimulation sites closer to our optimized location were more likely to yield positive responses. Furthermore, the E-field normal component induced by our optimized location in the targeted brain region was significantly higher

compared to the ADM method and the nearest scalp site. These results suggest that SEM-optimized coil placement may be more effective for TMS treatment and cognitive research.

Compared to previously published methods, such as the atlas of optimal coil orientation and position for TMS proposed by Gomez-Tames et al. [16] and the automated optimization method proposed by Lynch et al. [17], our SEM-based approach offers several advantages. Unlike the atlas-based approach, our SEM-based method considers individual differences in brain anatomy, resulting in more accurate targeting. Moreover, SEM-based optimization has been shown to enhance the repeatability and clinical effectiveness of TMS coil placement, which is crucial for clinical applications. Our approach also provides the convenience and generalizability of easy replication using our open-source software and offers an a priori method for optimizing individual coil placement.

In contrast to the automated optimization method proposed by Lynch et al. [17] which requires extensive pre-processing of individual MRI data, our SEM-based method offers a more practical and efficient approach. The need for extensive pre-processing can be a limitation in clinical settings where time and resources are often limited. By utilizing the SEM framework, we can achieve optimized coil placement without the need for extensive pre-processing, making our method more time-efficient and cost-effective for practical implementation in clinical settings. Furthermore, our SEM-based method has been tested for reproducibility, convenience, and applicability to a wide range of patients and clinical settings. It provides a standardized approach that ensures consistent and reliable results across different patients and clinical contexts.

In summary, our SEM-based method for optimizing coil placement represents a significant improvement over existing methods, offering enhanced efficacy and reproducibility in various clinical applications of TMS interventions.

4.3 SEM approves reproducible, convenient, and generalizable applications of optimized coil placement

We have applied the proposed SEM framework to construct an optimal coil placement and demonstrated its repeatability across three independent datasets, employing approximately 5 million simulations. This is consistent with previous studies that have utilized an optimization strategy based on simulated E-fields, yielding consistent results [12, 16, 20]. Constructing an optimal coil placement for brain targets is desirable due to the computational and labor-intensive nature of the simulation process. Our study provides a high-quality "standard" average stimulation effects-based optimal coil placement and demonstrates the repeatability of this placement.

The implications of our findings are significant for both clinical treatment and cognitive research, particularly regarding the use of the SEM-based optimization method for TMS coil placement. Our results indicate that the SEM-based optimization method has clinical interpretability, making it a valuable tool for optimizing TMS treatment in depression and other psychiatric disorders. Additionally, our study suggests that the SEM-based optimization method is a promising tool for optimizing coil positioning in TMS treatment and cognitive experiments, as it eliminates the need for further calculations and conversions and can result in greater energy concentration within the targeted cortical region, ultimately improving clinical outcomes. Therefore, the SEM-based optimization method has the potential to advance TMS research and clinical practice, benefiting patients with depression and other psychiatric disorders.

Furthermore, we confirmed that the SEM-based optimization method can increase the efficiency of individual coil placement optimization. By converting the HAC coordinates of optimal coil placements to MNI coordinates, these placements can be easily integrated into existing commercially available coil localizing devices, such as TMS neuronavigation or robotic systems. The SEM-based optimization method enables users to guide coil placement based on *a priori* knowledge of optimal coil placements. Moreover, this *a priori* knowledge is compatible with numerical modeling toolboxes of E-fields, enabling researchers to optimize individual coil placements using *a priori* assumptions about aggregative coil placements. As an example of optimizing individual coil placements, we conducted an individual optimization study using the *Simnibs* modeling toolbox (Supplementary method 1, Supplementary figure 10). Compared to traditional and ADM optimization strategies, our prior coil placements improved the efficiency of the optimization process and corresponded to greater stimulation effects.

As a result, we have developed an open-sourced SEM-building pipeline and group-level prior for optimal coil placement, facilitating more convenient, reproducible, and generalizable applications. Our findings underscore the potential of SEMs to enhance the accuracy and efficiency of TMS studies, leading to more effective clinical outcomes.

4.4 Extensibility of SEM construction for optimal coil placement

The extensibility of the SEM construction for optimal coil placement is not limited to specific stimulation targets but can be applied to any dataset that quantifies stimulation effects. This allows for potential extensions to suit various electrophysiological detection or modeling techniques. In this study, we focused on targeted regions of interest (ROIs) selected from a brain atlas, but it is worth noting that other brain atlases may offer valuable options for researchers. The generic nature of the SEM building strategy allows it to be applied to any target region with anatomical information. This can include *a priori* locations or subject-specific cortical targets delineated based on anatomical, functional, or meta-analytical information about neural circuits and brain networks [12, 17, 19, 32, 42].

Furthermore, the SEM construction framework can be built using different spatial and temporal stimulation effects revealed by neuroimaging techniques [reviewed in [9, 43]]. Various responses from different neuroimaging techniques could be utilized to define a specific evaluation function of the stimulation effect. For example, functional connectivity changes revealed by functional MRI data and the dynamic responses of EEG and MEG data can be used to evaluate the stimulation effects. This allows for the evaluation function of the SEM to be extended to assess the stimulation effects based on the spatiotemporal response characteristics across different brain scales, which contribute to the generation of macroscopic neuroimaging signals, including fMRI, EEG, and MEG.

In summary, the extensibility of the SEM construction for optimal coil placement is broad and can be applied to different datasets and techniques. It allows for flexibility in selecting targeted ROIs and evaluating stimulation effects based on various neuroimaging modalities. This versatility enhances the applicability and potential impact of the SEM framework in advancing TMS research and clinical practice.

5 Conclusion

In summary, the SEM framework presented in this study provides a reliable and effective method for mapping transcranial stimulation effects. The extensive simulations and validation of diverse datasets demonstrate the robustness and consistency of the SEM construction. The framework's effectiveness and stability were demonstrated in both retrospective TMS treatment data and a new healthy dataset, highlighting its applicability across different populations. The ability to aggregate neuromodulation data within the SEM framework opens up possibilities for meta-analyses of multiple studies conducted at various sites. This aggregation enhances statistical power and facilitates reproducible research outcomes. By offering a standardized approach to transcranial mapping, the SEM framework contributes to the advancement of precise transcranial neuromodulation techniques. Future research can build upon the SEM framework by exploring its application in different contexts and expanding its capabilities. This includes investigating its potential in other neuroimaging modalities, such as EEG and fMRI, and exploring its utility in clinical settings for personalized treatment interventions. The SEM framework holds promise for further enhancing our understanding of brain function and advancing the field of transcranial neuromodulation.

Acknowledgments

Declaration of interests: T.J. reports grants from the Science and Technology Innovation 2030 - Brain Science and Brain-Inspired Intelligence Project (Grant No. 2021ZD0200200), Natural Science Foundation of China (Grant Nos. 82151307 and 31620103905), Strategic Priority Research Program of the Chinese Academy of Sciences (Grant No. XDB32030207), and Science Frontier Program of the Chinese Academy of Sciences (Grant No. QYZDJ-SSW-SMC019), during the conduct of the study. The remaining authors reported no relevant conflicts.

Ethical Approval: All procedures performed in studies involving human participants were by the ethical standards of the institutional and national research committee and with the 1964 Helsinki Declaration and its later amendments or comparable ethical standards.

Acknowledgments: We are very grateful to all the participants who contributed to this article. R. E. Perozzi and E. F. Perozzi assisted with English language and editing.

Authors' Contributions: T.J. proposed the concept and designed the protocol. G.Z. performed the concept and analyzed data. L.M. and Y.Y. performed the experiments, and B.Z. performed the MRI scanning. D.C., J.L., and N.Z. contributed to the data analysis. T.J., Z.Y., and L.F. led the project and supervised the experiments. All authors contributed to the writing of the manuscript. Data access and verification: G.Z., L.M., and Y.Y.

Fundings: This work was partially supported by grants from the Science and Technology Innovation 2030 - Brain Science and Brain-Inspired Intelligence Project (Grant No. 2021ZD0200200), Natural Science Foundation of China (Grant Nos. 82151307 and 31620103905), Strategic Priority Research Program of the Chinese Academy of Sciences (Grant No. XDB32030207), and Science Frontier Program of the Chinese Academy of Sciences (Grant No. QYZDJ-SSW-SMC019).

References

[1] McClintock SM, Reti IM, Carpenter LL, et al. Consensus recommendations for the clinical application of repetitive transcranial magnetic stimulation (rtms) in the treatment of depression. J Clin Psychiatry, 2018, 79:

[2] Ni Z, Chen R. Transcranial magnetic stimulation to understand pathophysiology and as potential treatment for neurodegenerative diseases. Transl Neurodegener, 2015, 4: 22

[3] Walsh V, Cowey A. Transcranial magnetic stimulation and cognitive neuroscience. Nat Rev Neurosci, 2000, 1: 73-79

[4] Hallett M. Transcranial magnetic stimulation: A primer. Neuron, 2007, 55: 187-199

[5] Hallett M. Transcranial magnetic stimulation and the human brain. Nature, 2000, 406: 147-150

[6] Barker AT, Jalinous R, Freeston IL. Non-invasive magnetic stimulation of human motor cortex. The Lancet, 1985, 325: 1106-1107

[7] Trapp NT, Bruss J, King Johnson M, et al. Reliability of targeting methods in tms for depression: Beam f3 vs. 5.5 cm. Brain Stimulation, 2020, 13: 578-581

[8] Klem GH, Lüders HO, Jasper HH, et al. The ten-twenty electrode system of the international federation. The international federation of clinical neurophysiology. Electroencephalogr Clin Neurophysiol Suppl, 1999, 52: 3-6

[9] Cash RFH, Weigand A, Zalesky A, et al. Using brain imaging to improve spatial targeting of transcranial magnetic stimulation for depression. Biol Psychiatry, 2021, 90: 689-700

[10] Fitzgerald PB. Targeting repetitive transcranial magnetic stimulation in depression: Do we really know what we are stimulating and how best to do it? Brain Stimulation, 2021, 14: 730-736

[11] Numssen O, van der Burght CL, Hartwigsen G. Revisiting the focality of non-invasive brain stimulation - implications for studies of human cognition. Neurosci Biobehav Rev, 2023, 149: 105154

[12] Balderston NL, Beer JC, Seok D, et al. Proof of concept study to develop a novel connectivity-based electric-field modelling approach for individualized targeting of transcranial magnetic stimulation treatment. Neuropsychopharmacology, 2022, 47: 588-598

[13] Deng Z-D, Argyelan M, Miller J, et al. Electroconvulsive therapy, electric field, neuroplasticity, and clinical outcomes. Mol Psychiatry, 2022, 27: 1676-1682

[14] Suen PJC, Doll S, Batistuzzo MC, et al. Association between tdcs computational modeling and clinical outcomes in depression: Data from the elect-tdcs trial. Eur Arch Psychiatry Clin Neurosci, 2021, 271: 101-110

[15] Argyelan M, Oltedal L, Deng Z-D, et al. Electric field causes volumetric changes in the human brain. Elife, 2019, 8:

[16] Gomez-Tames J, Hamasaka A, Laakso I, et al. Atlas of optimal coil orientation and position for tms: A computational study. Brain stimulation, 2018, 11: 839-848

[17] Lynch CJ, Elbau IG, Ng TH, et al. Automated optimization of tms coil placement for personalized functional network engagement. Neuron, 2022,

[18] Weise K, Numssen O, Kalloch B, et al. Precise motor mapping with transcranial magnetic stimulation. Nat Protoc, 2022,

[19] Balderston NL, Roberts C, Beydler EM, et al. A generalized workflow for conducting electric field-optimized, fmri-guided, transcranial magnetic stimulation. Nat Protoc, 2020, 15: 3595-3614

[20] Gomez LJ, Dannhauer M, Peterchev AV. Fast computational optimization of tms coil placement for individualized electric field targeting. Neuroimage, 2021, 228: 117696

[21] Nielsen JD, Madsen KH, Puonti O, et al. Automatic skull segmentation from mr images for realistic volume conductor models of the head: Assessment of the state-of-the-art. Neuroimage, 2018, 174: 587-598

[22] Htet AT, Noetscher GM, Burnham EH, et al. Collection of sixteen high-quality human head cad models generated with simnibs 2.1 using connectome subject data within matlab® platform. bioRxiv, 2018, 480103

[23] Van Essen DC, Ugurbil K, Auerbach E, et al. The human connectome project: A data acquisition perspective. Neuroimage, 2012, 62: 2222-2231

[24] Glasser MF, Sotiropoulos SN, Wilson JA, et al. The minimal preprocessing pipelines for the human connectome project. Neuroimage, 2013, 80: 105-124

[25] Thielscher A, Antunes A, Saturnino GB. Field modeling for transcranial magnetic stimulation: A useful tool to understand the physiological effects of tms? Annu Int Conf IEEE Eng Med Biol Soc, 2015, 2015: 222-225

[26] Fan L, Li H, Zhuo J, et al. The human brainnetome atlas: A new brain atlas based on connectional architecture. Cereb Cortex, 2016, 26: 3508-3526

[27] George MS, Wassermann EM, Kimbrell TA, et al. Mood improvement following daily left prefrontal repetitive transcranial magnetic stimulation in patients with depression: A placebo-controlled crossover trial. Am J Psychiatry, 1997, 154: 1752-1756

[28] O'Reardon JP, Solvason HB, Janicak PG, et al. Efficacy and safety of transcranial magnetic stimulation in the acute treatment of major depression: A multisite randomized controlled trial. Biol Psychiatry, 2007, 62: 1208-1216

[29] Herwig U, Fallgatter AJ, Höppner J, et al. Antidepressant effects of augmentative transcranial magnetic stimulation: Randomised multicentre trial. The British Journal of Psychiatry : the Journal of Mental Science, 2007, 191: 441-448

[30] Rusjan PM, Barr MS, Farzan F, et al. Optimal transcranial magnetic stimulation coil placement for targeting the dorsolateral prefrontal cortex using novel magnetic resonance image-guided neuronavigation. Hum Brain Mapp, 2010, 31: 1643-1652

[31] Mir-Moghtadaei A, Caballero R, Fried P, et al. Concordance between beamf3 and mri-neuronavigated target sites for repetitive transcranial magnetic stimulation of the left dorsolateral prefrontal cortex. Brain Stimul, 2015, 8: 965-973

[32] Herbsman T, Avery D, Ramsey D, et al. More lateral and anterior prefrontal coil location is associated with better repetitive transcranial magnetic stimulation antidepressant response. Biol Psychiatry, 2009, 66: 509-515

[33] Nathou C, Simon G, Dollfus S, et al. Cortical anatomical variations and efficacy of rtms in the treatment of auditory hallucinations. Brain Stimulation, 2015, 8: 1162-1167

[34] Zhang BBB, Stöhrmann P, Godbersen GM, et al. Normal component of tms-induced electric field is correlated with depressive symptom relief in treatment-resistant depression. Brain Stimulation, 2022, 15: 1318-1320

[35] Okamoto M, Dan H, Sakamoto K, et al. Three-dimensional probabilistic anatomical cranio-cerebral correlation via the international 10-20 system oriented for transcranial functional brain mapping. Neuroimage, 2004, 21: 99-111

[36] Jurcak V, Tsuzuki D, Dan I. 10/20, 10/10, and 10/5 systems revisited: Their validity as relative head-surface-based positioning systems. Neuroimage, 2007, 34: 1600-1611

[37] Tsuzuki D, Watanabe H, Dan I, et al. Minr 10/20 system: Quantitative and reproducible cranial landmark setting method for mri based on minimum initial reference points. J Neurosci Methods, 2016, 264: 86-93

[38] Xiao X, Yu X, Zhang Z, et al. Transcranial brain atlas. Sci Adv, 2018, 4: eaar6904

[39] Jiang Y, Du B, Chen Y, et al. A scalp-measurement based parameter space: Towards locating tms coils in a clinically-friendly way. Brain Stimulation, 2022, 15: 924-926

[40] Cardenas VA, Bhat JV, Horwege AM, et al. Anatomical and fmri-network comparison of multiple dlpfc targeting strategies for repetitive transcranial magnetic stimulation treatment of depression. Brain Stimulation, 2022, 15: 63-72

[41] Bungert A, Antunes A, Espenhahn S, et al. Where does tms stimulate the motor cortex? Combining electrophysiological measurements and realistic field estimates to reveal the affected cortex position. Cereb Cortex, 2017, 27: 5083-5094

[42] Siddiqi SH, Taylor SF, Cooke D, et al. Distinct symptom-specific treatment targets for circuit-based neuromodulation. Am J Psychiatry, 2020, 177: 435-446

[43] Zhong G, Yang Z, Jiang T. Precise modulation strategies for transcranial magnetic stimulation: Advances and future directions. Neuroscience Bulletin, 2021, 37: 1718-1734